Rapid Communication

Tairong Kuang, Runhang Zeng, Aleksander Hejna, Mohammad Reza Saeb, Bozhen Wu*, Feng Chen, Tong Liu*, and Mingqiang Zhong

Pressure-induced flow processing behind the superior mechanical properties and heat-resistance performance of poly(butylene succinate)

https://doi.org/10.1515/epoly-2022-0018
received November 24, 2021; accepted December 25, 2021

Abstract: We propose a pressure-induced flow (PIF) processing method for the simultaneous enhancement of strength, toughness, and heat resistance of biodegradable poly(butylene succinate) (PBS). The pressure and temperature were systematically adjusted to optimize the tensile strength of PBS. Under the optimized processing conditions, the structured PBS was characterized by relatively high strength of 89.5 MPa, toughness of 21.4 kJ·m^{-2}, and improved heat resistance without deterioration of much of its ductility. Microscopic analyses witnessed denser and highly oriented crystalline domains along the flow direction caused by PIF processing. Detailed crystallization analysis made by 2D-WAXD and 2D-SAXS unraveled the extremely ordered PBS domains, which were featured by a significant increase in the orientation degree from 0.25 for the reference to 0.73 for PIF-processed PBS. Such a highly ordered microstructure substantially boosted the degree of crystallinity and heat-resistance temperature of PBS. We believe that our findings would offer a facile, green, and cost-effective approach for fabricating biodegradable polymers with outstanding properties and performance.

Keywords: poly(butylene succinate), pressure-induced flow, mechanical properties, crystallization, heat resistance

*** Corresponding author: Bozhen Wu,** College of Material Science and Engineering, Zhejiang University of Technology, Hangzhou, 310014, China, e-mail: wubz_314@163.com
*** Corresponding author: Tong Liu,** College of Material Science and Engineering, Zhejiang University of Technology, Hangzhou, 310014, China, e-mail: liut@zjut.edu.cn
Tairong Kuang, Runhang Zeng, Feng Chen, Mingqiang Zhong: College of Material Science and Engineering, Zhejiang University of Technology, Hangzhou, 310014, China
Aleksander Hejna, Mohammad Reza Saeb: Department of Polymer Technology, Faculty of Chemistry, Gdańsk University of Technology, Narutowicza 11/12, 80-233 Gdańsk, Poland

Over the last two decades, policymakers and governments have been asked for a paradigm shift in manufacturing plastics from fossil-based to biodegradable polymers (1,2). Poly(butylene succinate) (PBS) can be named as a biodegradable polymer with many favorable features, including balanced thermal and mechanical performance, low cost, good processability, as well as good chemical resistance (3,4). However, it suffers from insufficient mechanical properties and a thermal-sensitive crystallization mechanism. The proposed solutions to reinforce PBS are mainly based on different modification methods, such as copolymerization (5), chain extension (6), cross-linking (7), and blending (8). For instance, comonomers of different classes may compensate for the brittleness and thermal sensitivity of PBS through tailor-making PBS backbone, but such treatment deteriorates the crystallinity and tensile strength (9). Chain extension or cross-linking has also been examined to improve the heat resistance and melt strength of PBS (6,7,10). In addition, blending with natural or biodegradable polymers and micro/nanofillers was also effective in improving the toughness of PBS (11,12).

Although modifications like blending with secondary polymers or using a comonomer in polymerization could significantly enhance some properties of PBS, improving the tensile strength and toughness, such modifications were inadequate for practical usage. Moreover, some drawbacks are frequently associated with these strategies, such as the loss of biocompatibility and biodegradability upon additive incorporation, difficulties in processing methods, and costly operation arising from blending PBS with reinforcing components. To combat such deficiencies, we propose

a pressure-induced flow (PIF) processing approach, in which the pressure is exerted on the PBS in a semi-solid state to directly strengthen and toughen PBS without the need for further treatment. We have already proved that PIF processing is an easy, green, and cost-effective method to enhance the semi-crystalline polymers' tensile strength and toughness (13–16). However, there is no information about the effect of PIF processing on the crystallization and thermomechanical properties of PBS. Herein we examine the effect of processing temperature and pressure on the microstructure, thermal, and mechanical properties of PBS. The crystalline structures were imaged on a scanning electron microscope (SEM), followed by detailed crystallographic analyses using 2D small-angle X-ray scattering (2D-SAXS), and 2D wide-angle X-ray diffraction (2D-WAXD). Eventually, significant changes in the tensile strength and toughness aided by PIF processing were discussed through the lens of crystallization and thermal phenomena.

The tensile strength of PBS prepared under different processing conditions is shown in Figure 1a and Table A1 (in the Appendix). Obviously, the tensile strength of the PIF PBS sample is significantly higher than that of the sample obtained by conventional injection molding (CIM). Under all PIF processing conditions, the tensile strength of PIF samples increased with the increase of the processing temperature and pressure. When the processing temperature was low (40°C), the tensile strength of PIF samples depended significantly on the exerted pressure, and the relationship was almost linear. As the processing temperature increased, the tensile strength was less sensitive to the exerted pressure changes. When the processing temperature was 80°C, the influence of the exerted pressure was hardly significant over 100 MPa. The further increase did not contribute significantly to the tensile strength of the samples. This was because when PIF processing was performed at a lower temperature, the flowability of the samples was still poor despite exceeding the glass transition temperature of PBS (around −30°C). The increase in the exerted pressure could induce large deformation of the polymer aggregation structure (17). With the increase in processing temperature, the mobility of the PBS chain

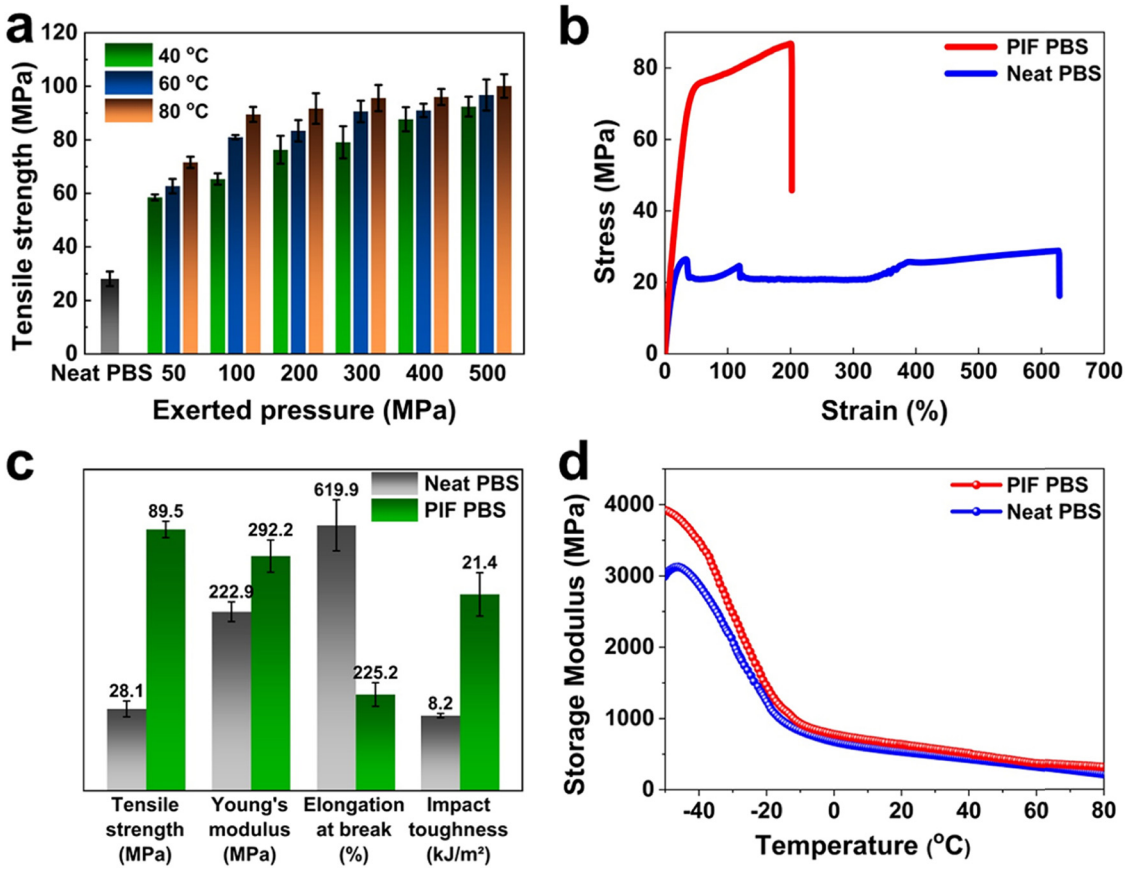

Figure 1: Mechanical properties of neat PBS and PIF PBS: (a) tensile properties of the samples under various processing conditions; (b) stress–strain curves; (c) detailed comparison analysis of mechanical properties; (d) storage modulus.

segments increased significantly, leading to a significant increase in PBS ductility and higher orientation during PIF processing. Moreover, the high degree of orientation of the chain segments along the flow direction also promoted the orientation and recrystallization of PBS. Further, through error analysis, the performance stability of samples processed by PIF processing at lower exerted pressures was higher than that of samples processed at higher exerted pressures. This was because the higher exerted pressures were accompanied by a higher degree of orientation, slippage of polymer chains, and interlayer slippage, which are more likely to accumulate defects (18).

Considering that the high pressure would affect the equipment requirements, energy consumption, maintenance costs, and safety issues in actual production, 80°C and 100 MPa were selected as the preferred PIF processing conditions in this work. As shown in Figure 1b, the stress–strain curves of PIF PBS samples became smoother and steeper than that of the neat PBS, and no significant fluctuations were observed. This indicated that the internal morphological structure of the samples was more homogeneous and less defective after PIF processing. After PIF processing, the tensile strength and Young's modulus of PIF PBS samples reached 89.5 and 292.2 MPa, respectively, 218.5% and 31.1% higher than those of neat PBS. Also, the elongation at break of the PIF PBS sample remained above 220% (Figure 1c). However, due to the orientation of macromolecules during PIF processing, the possibility for elongation during tension was decreased, so the final elongation accounted only for 36% of the initial PBS value. The toughness results showed that the impact strength of PIF PBS could reach 21.4 $kJ \cdot m^{-2}$, which was about 2.6 times higher than that of the neat PBS (Figure 1c). The dynamic mechanical analysis (DMA) results of neat PBS and PIF PBS are shown in Figure 1d. The PIF PBS sample showed significantly higher storage modulus in the low-temperature region than that of neat PBS. In contrast, the difference in storage modulus gradually decreased with the increase of temperature, consistent with the tensile modulus results obtained at room temperature. In summary, the strength, modulus, and impact toughness of PBS were significantly improved after PIF processing under appropriate conditions while maintaining the high elongation at break, which means that the PIF process could achieve simultaneous strengthening and toughening of PBS.

The changes in the properties of polymeric materials are inevitably caused by their structural changes. Thus,

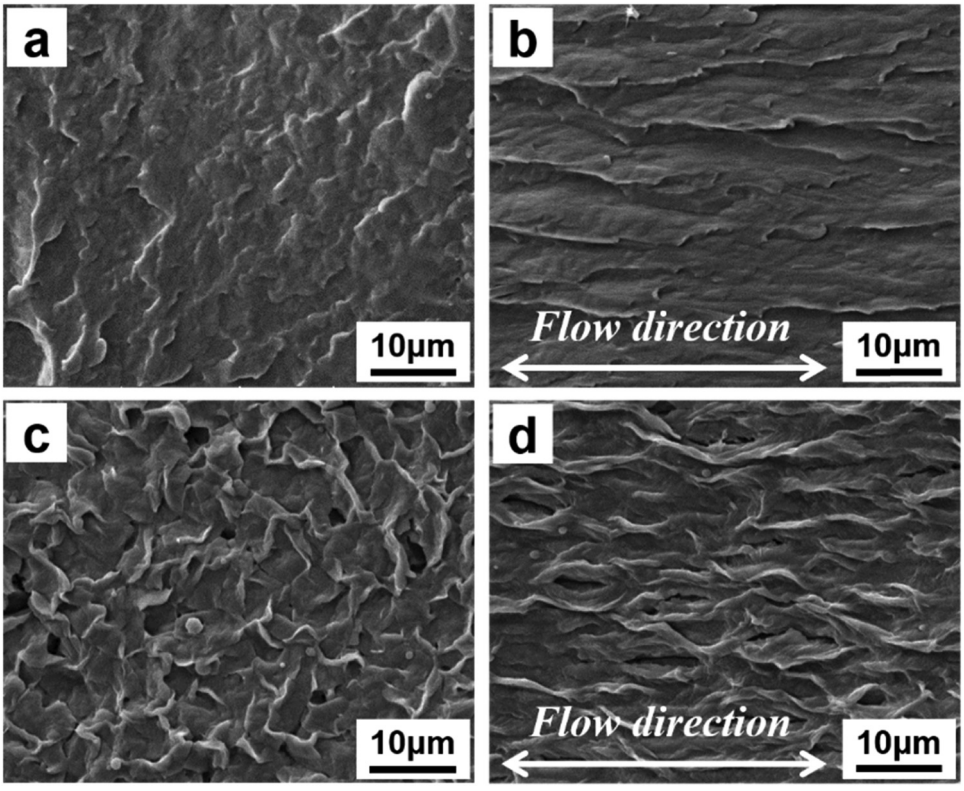

Figure 2: The cryo-fracture surfaces of (a) neat PBS and (c) PIF PBS; crystal morphology of (b) neat PBS and (d) PIF PBS.

SEM was used to investigate the effect of the PIF process on the microstructure of neat PBS and PIF PBS samples. The brittle-fracture cross-sectional SEM micrographs of the samples are presented in Figure 2a and c. Neat PBS exhibits a smooth fracture surface, while the PIF PBS sample presents noticeable orientation features along the flow direction. To further determine the crystalline structure of PBS before and after PIF processing, an etching process was carried out on the brittle-fracture cross-section of the samples to remove the amorphous regions. The crystalline structures after etching are presented in Figure 2b and d. The lamellae in the neat PBS were disordered, while the crystals in the matrix were oriented in the flow direction and became denser after the PIF processing. Moreover, the lamella bundles became oriented in the flow direction and formed an interconnected structure between the lamellar crystals. It has been shown in previous studies that the spherical crystal boundaries were the stress weak points (19). The PIF process was accompanied by the deformation, fragmentation, and rearrangement of the spherical crystals to form an ordered lamellae, which was beneficial to improving the samples' mechanical properties. In this work, after PIF processing, the crystalline structure of PBS changed from disordered lamellae to a highly ordered interconnected crystalline structure, which was beneficial to improve the tensile and impact properties of the samples simultaneously.

To further evaluate the molecular and crystal orientation of PBS after PIF processing, 2D-WAXD and 2D-SAXS techniques were used, and the results are shown in Figure 3. It can be found that the crystalline structure and molecular orientation of PBS materials changed significantly after PIF processing. The 2D-SAXS pattern of the neat PBS sample showed almost isotropic circles, indicating a randomly oriented lamellar morphology. After PIF processing, an obvious earlobe scattering signal can be observed in the equatorial direction of the 2D-SAXS pattern, implying that some of the lamellar structures and molecular chains in the samples are oriented along the flow direction (Figure 3a and b). The diffraction signals of the (110) and (020) planes of α-crystalline PBS can be observed from the 2D-WAXD pattern (Figure 3c and d) (20,21). The diffraction pattern of neat PBS still shows an isotropic ring with uniform intensity distribution, which implies a random orientation of PBS crystals. The results are consistent with the 2D-SAXS. In contrast, the PIF PBS sample showed a divergence in signal intensity and extreme values in the meridian for each plane. The signal intensity along the flow direction was much greater than that in the vertical direction, indicating that PIF processing led to the high orientation of molecular chains and crystals. To quantitatively compare the effect of PIF processing on the degree of orientation of the samples, 1D-WAXD curves were obtained from 2D-WAXD patterns by circular integration in Figure 3e, and the calculated orientation degree from the (110) plane is shown in the inset (Figure 3e). The results show that the orientation degree of the PIF PBS sample was increased from 0.25 of neat PBS to 0.73. The substantial increase in the orientation degree is highly consistent with the SEM's fracture morphology and crystalline structure.

According to the signal intensities of 2D-WAXD and 2D-SAXS patterns results, it should be noted that PIF processing resulted in not only a highly oriented molecular chain and crystalline structure but also a significant increase in crystallinity. To quantitatively study the effect of PIF processing on the crystallinity and melting temperature of PBS, differential scanning calorimetry (DSC) tests were conducted and the results are shown in Figure 4a. It is observed that neat PBS exhibits two endothermic

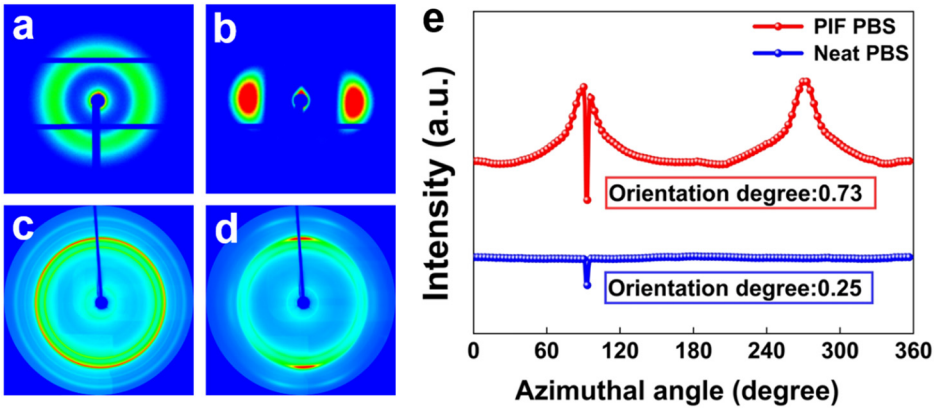

Figure 3: 2D-SAXS patterns of (a) neat PBS and (b) PIF PBS; 2D-WAXD patterns of (c) neat PBS and (d) PIF PBS; (e) the 1D-WAXD curves of neat PBS and PIF PBS.

melting peaks caused by the imperfect crystallization of PBS during the CIM process. The imperfect and finely divided crystals melt and absorb heat first when the temperature increases to about 85°C, and the more perfect crystals start to melt. Unlike the neat PBS, the PIF PBS sample shows only one broader melting peak in the DSC curve, and the melting point slightly shifts to a higher temperature (from 107°C to 108.8°C), indicating that the PIF processing makes the crystallization of PBS more perfect, which is attributed to higher orientation of the structure. The crystallinity of the samples was calculated by integrating the area under the melting endotherms from the DSC curve, and the equation is

$$X_c = \frac{\Delta H_m}{\Delta H_m^0} \times 100\% \quad (1)$$

where ΔH_m is the enthalpy of fusion and ΔH_m^0 is the melting enthalpy of the perfect crystal (110.3 J·g^{-1}). It should be noted that the crystallinity of PBS significantly increased from 18.1% of neat PBS to 30.2% of PIF PBS. After PIF processing, not only the orientation of the PBS sample was significantly increased, but the more perfect crystal structure formed led to the improved crystallinity and melting temperature, which is essential to increase the service temperature of the PBS material. Therefore, we put the neat PBS and PIF PBS samples into the oven for hot air treatment to evaluate the heat resistance. Figure 4b shows that both samples were treated at 40°C for 2 h without deformation. After being treated at 100°C for 2 h, the PIF PBS sample could maintain the initial shape and size, while the neat PBS had obvious deformation. This result suggests that the PIF processing improves the internal morphological structure of PBS and can effectively improve the heat resistance of the materials.

We have successfully prepared high-performance PBS materials through PIF processing. The tensile strength and tensile modulus increased by ca. 219% and 31% compared with neat PBS, respectively, and the elongation at break kept still high (~225.2%), despite the reduced ductility. At the appropriate processing conditions, the impact toughness enhanced significantly from 8.2 (neat PBS) to 21.4 kJ·m^{-2}. PIF processing has fully contributed to improving strength and toughness because of the formation of a highly oriented crystalline structure, as demonstrated by the SEM, 2D-SAXS, and 2D-WAXD results. Thermal properties corresponding to T_m and X_c of the PIF PBS sample were improved to 108.8°C and 30.2%, respectively. Overall, the high-performance PBS material prepared by a simple, green, and low-cost approach can potentially replace petroleum-based/non-degradable polymer in high-performance and high value-added fields. In further works, a more comprehensive investigation of the PIF process parameters would be performed along with the analysis of their impact on the ecological and economic aspects of the process.

Experimental

Materials

PBS (Bionolle 1903MD) was purchased from Showa Denko, Japan. It has a density of 1.26 g·cm^{-3} and a melt flow index of 4.5 g·10 min^{-1} (190°C, 2.16 kg). The raw materials were used without pretreatment.

Preparation of structured PBS samples

PBS pellets were first dried in an oven at 70°C for 12 h to remove moisture and prevent degradation of the molecular

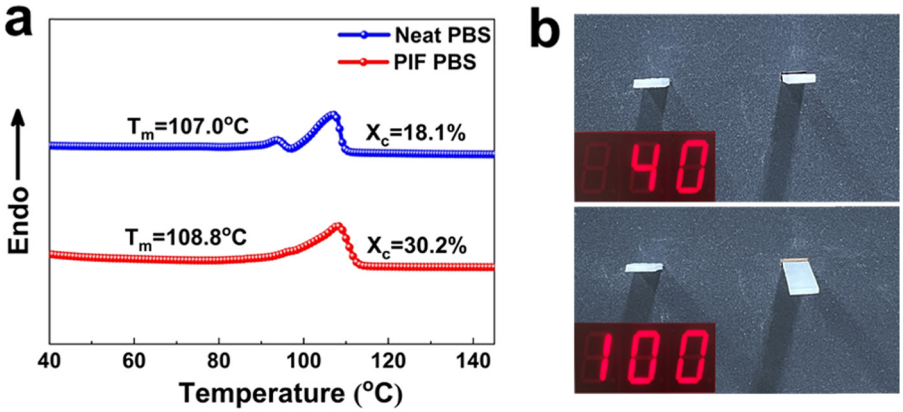

Figure 4: (a) Thermal properties of the samples: DSC heating curve of neat PBS and PIF PBS; (b) digital photo of neat PBS and PIF PBS treated in a hot air atmosphere at 40°C and 100°C for 2 h, respectively.

chains caused by melt processing. The dried PBS pellets were processed by CIM, and the barrel, nozzle, and mold temperatures in the injection molding process were set in the range of 130–160°C. Subsequently, the obtained dumbbell-shaped samples were cut to the rectangular shape of 30 $mm^3 \times 10$ $mm^3 \times 4$ mm^3 for the subsequent processing. Finally, the rectangular PBS samples were further processed by PIF processing. The schematic diagram of the PIF mold is shown in Figure 5. In this study, to investigate the effect of processing parameters on the microstructure and properties of PBS materials, the orthogonal tests were conducted with two parameters, i.e., PIF temperature was set to 40°C, 60°C, and 80°C, and pressure was set to 50, 100, 200, 300, 400, and 500 MPa, respectively.

Characterization

Mechanical properties

Tensile properties of CIM and PIF samples were tested using a universal mechanical testing instrument (Instron 5966, USA). Tensile tests were carried out at a 10 $mm \cdot min^{-1}$ tensile rate. Notched lzod impact strength was tested by a XC-22 impact tester (Chengde, China).

DSC

The melting behavior of CIM and PIF samples was determined using DSC (Mettler Toledo, Switzerland). For the CIM sample, the samples were initially heated to 150°C to eliminate thermal history and held at this temperature for 5 min; then, the samples were cooled to 30°C and again heated to 150°C. The DSC test under a nitrogen atmosphere was performed for the PIF sample from room temperature to 150°C. All the heating rate or cooling rate was 10°C·min^{-1}.

DMA

The DMA properties of CIM and PIF samples were analyzed using a dynamic mechanical analyzer (Q800, TA Instruments Company, USA) with a single cantilever mode. The heating rate was 3°C·min^{-1} and the frequency was 1 Hz.

SEM

The fracture surface and crystal morphology of CIM and PIF samples were observed under an SEM (VEGA3 SBH-EasyProbe, TESCAN, Czech Republic). The brittle fracture surfaces were obtained by immersing the samples in liquid nitrogen for 1 h, followed by a rapid brittle fracture in the flow direction. To investigate the effect of PIF processing on the crystal morphology, the brittle fracture surfaces of the above samples were placed in a 1 mol·L^{-1} sodium hydroxide solution (solvent is a mixture of methanol and water in equal volume) and mechanically stirred at 30°C for 12 h to remove the amorphous regions. After that, the surface of the samples was cleaned using deionized water. Before SEM observation, the samples were subject to spray gold treatment.

2D SAXS/WAXD

The molecular and crystal orientation of neat PBS and PIF PBS samples were determined by 2D-WAXD and 2D-SAXS at the beamline BL15U1 and BL16B1 in the Shanghai

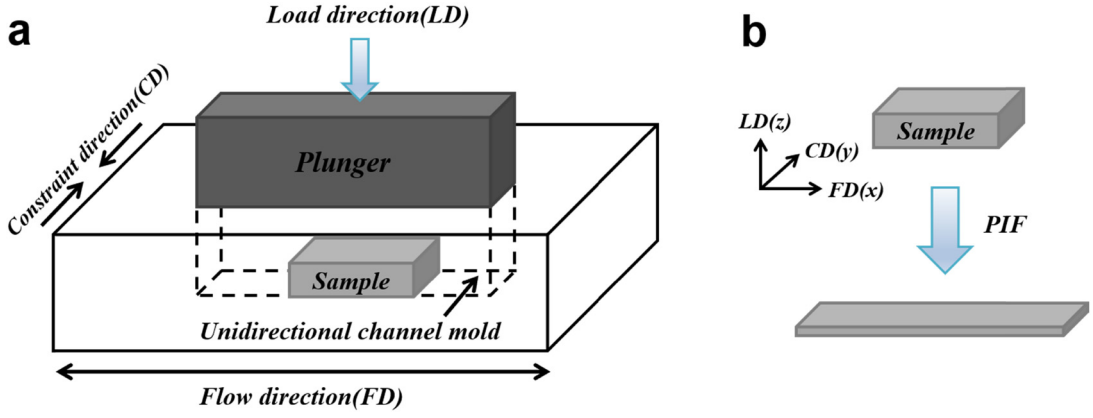

Figure 5: Schematic diagram of (a) PIF processing, (b) shape change.

Synchrotron Radiation Facility (SSRF, Shanghai, China). For the 2D-WAXD test, the X-ray energy, wavelength, spot size, and the distance between the specimen and detector were 10 keV, 0.124 nm, 3.0 $\mu m^2 \times 2.5\ \mu m^2$, and 170 mm, respectively. For the 2D-SAXS test, the X-ray energy, wavelength, spot size, and the distance between the specimen and detector were 10 keV, 0.124 nm, 174 $\mu m^2 \times 372\ \mu m^2$, 1,860 mm, respectively. The 2D-WAXD results were further used to calculate the orientation parameter using a weighted average of orientation factor $f(\varphi)$ from the (110) plane:

$$f(\varphi) = \frac{3(\cos^2\varphi) - 1}{2} \tag{2}$$

and

$$\langle f(\varphi)\rangle = \frac{\int_0^{\pi} f(\varphi) I(\varphi) \mathrm{d}\varphi}{\int_0^{\pi} I(\varphi) \mathrm{d}\varphi} \tag{3}$$

where φ is the azimuthal angle and $I(\varphi)$ is the scattered intensity along the angle φ.

Acknowledgements: We thank the support of the National Natural Science Foundation of China (No. 51803062, 52173046, 51873193, and 52173086), Natural Science Foundation of Zhejiang Province (No. LZ21E030002), Natural Science Foundation of Guangdong Province (No. 2019A1515012125), Shandong Provincial Key Research and Development Plan (Major Science and Technology Innovation Project) (No. 2020CXGC010312), Ningbo Scientific and Technological Innovation 2025 Major Project (No. 2020Z097), and the Fundamental Research Funds for the Provincial Universities of Zhejiang (No. RF-A2020008). We also acknowledge BL15U1 and BL16B1 beamlines in the Shanghai Synchrotron Radiation Facility (SSRF, Shanghai, China) for the kind help on the X-ray measurements.

Author contributions: Tairong Kuang: investigation, conceptualization, methodology, writing – original draft, writing – review and editing, supervision; Runhang Zeng: investigation, formal analysis; Aleksander Hejna: formal analysis, writing – review and editing; Mohammad Reza Saeb: writing – review and editing; Bozhen Wu: formal analysis, supervision; Feng Chen: formal analysis, supervision; Tong Liu: investigation, writing – original draft, supervision; Mingqiang Zhong: supervision.

Conflict of interest: The authors state no conflict of interest.

Data availability statement: The datasets generated during and/or analyzed during the current study are available from the corresponding author on reasonable request.

References

(1) Kuang TR, Ju J, Liu T, Hejna A, Saeb MR, Zhang S, et al. A facile structural manipulation strategy to prepare ultra-strong, super-tough, and thermally stable polylactide/nucleating agent composites. Adv Compos Hybrid Mater. 2022. doi: 10.1007/s42114-021-00390-2

(2) Zhang Q, Song M, Xu Y, Wang W, Wang Z, Zhang L. Bio-based polyesters: recent progress and future prospects. Prog Polym Sci. 2021;120:101430.

(3) Hu X, Li Y, Gao Y, Wang R, Wang Z, Kang H, et al. Renewable and super-toughened poly(butylene succinate) with bio-based elastomers: preparation, compatibility and performances. Eur Polym J. 2019;116:438–44.

(4) Xu Y, Zhang S, Peng X, Wang J. Fabrication and mechanism of poly(butylene succinate) urethane ionomer microcellular foams with high thermal insulation and compressive feature. Eur Polym J. 2018;99:250–8.

(5) Hwang SY, Yoo ES, Im SS. The synthesis of copolymers, blends and composites based on poly(butylene succinate). Polym J. 2012;44(12):1179–90.

(6) Lv L, Wu F, Chen S-C, Wang Y-Z, Zeng J-B. Properties regulation of poly(butylene succinate) ionomers through their ionic group distribution. Polymer. 2015;66:148–59.

(7) Liu G-C, Zhang W-Q, Wang X-L, Wang Y-Z. Synthesis and performances of poly(butylene-succinate) with enhanced viscosity and crystallization rate via introducing a small amount of diacetylene groups. Chin Chem Lett. 2017;28(2):354–7.

(8) Roy N, Sengupta R, Bhowmick AK. Modifications of carbon for polymer composites and nanocomposites. Prog Polym Sci. 2012;37(6):781–819.

(9) Xu J, Guo B-H. Poly(butylene succinate) and its copolymers: Research, development and industrialization. Biotechnol J. 2010;5(11):1149–63.

(10) Jin H-J, Kim D-S, Lee B-Y, Kim M-N, Lee I-M, Lee H-S, et al. Chain extension and biodegradation of poly(butylene succinate) with maleic acid units. J Polym Sci Part B: Polym Phys. 2000;38(17):2240–6.

(11) Tsi H-Y, Tsen W-C, Shu Y-C, Chuang F-S, Chen C-C. Compatibility and characteristics of poly(butylene succinate) and propylene-co-ethylene copolymer blend. Polym Test. 2009;28(8):875–85.

(12) Zeng R-T, Hu W, Wang M, Zhang S-D, Zeng J-B. Morphology, rheological and crystallization behavior in non-covalently functionalized carbon nanotube reinforced poly(butylene succinate) nanocomposites with low percolation threshold. Polym Test. 2016;50:182–90.

(13) Kuang T, Chen F, Fu D, Chang L, Peng X, Lee LJ. Enhanced strength and foamability of high-density polyethylene prepared by pressure-induced flow and low-temperature cross-linking. RSC Adv. 2016;6(41):34422–7.

(14) Fu D, Kuang T, Chen F, Lee LJ, Peng X. Fabrication of high strength PA6/PP blends with pressure-induced-flow processing. Mater Chem Phys. 2015;164:1–5.

(15) Li D, Fu D, Yen Y-C, Benatar A, Peng X, Chiu DY, et al. Ultrasound-assisted-pressure-induced-flow leading to superior polymer/carbon nanotube composites and foams. Polymer. 2015;80:237–44.
(16) Fu D, Chen F, Peng X, Kuang T. Polyamide 6 modified polypropylene with remarkably enhanced mechanical performance, thermal properties, and foaming ability via pressure-induced-flow processing approach. Adv Polym Technol. 2018;37(8):2721–9.
(17) Ojijo V, Sinha Ray S, Sadiku R. Toughening of biodegradable polylactide/poly(butylene succinate-co-adipate) blends via in situ reactive compatibilization. ACS Appl Mater Interfaces. 2013;5(10):4266–76.
(18) Chen X, Galeski A, Michler GH. Morphological alteration and strength of polyamide 6 subjected to high plane–strain compression. Polymer. 2006;47(9):3171–85.
(19) Galeski A. Strength and toughness of crystalline polymer systems. Prog Polym Sci. 2003;28(12):1643–99.
(20) Wang K, Jiao T, Wang Y, Li M, Li Q, Shen C. The microstructures of extrusion cast biodegradable poly(butylene succinate) films investigated by X-ray diffraction. Mater Lett. 2013;92:334–7.
(21) Xie L, Xu H, Niu B, Ji X, Chen J, Li Z-M, et al. Unprecedented access to strong and ductile poly(lactic acid) by introducing in situ nanofibrillar poly(butylene succinate) for green packaging. Biomacromolecules. 2014;15(11):4054–64.

Appendix

Table A1: Tensile properties of the neat PBS and PIF-processed PBS samples under various processing conditions

Sample	Tensile strength MPa	Young's modulus MPa	Elongation at break %
Neat PBS	28.1 ± 2.7	222.9 ± 22.1	619.9 ± 59.4
PIF-40-50	58.5 ± 1.1	220.3 ± 7.1	349.7 ± 14.4
PIF-40-100	65.4 ± 3.1	223.3 ± 17.3	264.2 ± 45.2
PIF-40-200	76.3 ± 5.2	224.6 ± 24.1.	231.8 ± 25.6
PIF-40-300	76.1 ± 10.1	222.2 ± 27.8	224.3 ± 47.7
PIF-40-400	87.7 ± 4.5	300.0 ± 15.2	213.1 ± 4.4
PIF-40-500	92.4 ± 3.7	265.4 ± 26.8	235.1 ± 12.2
PIF-60-50	62.7 ± 2.7	240.3 ± 11.4	297.0 ± 27.4
PIF-60-100	79.0 ± 6.0	244.1 ± 1.6	232.8 ± 2.6
PIF-60-200	80.3 ± 4.6	231.9 ± 33.1	237.7 ± 22.0
PIF-60-300	90.6 ± 4.0	261.8 ± 19.0	222.8 ± 10.4
PIF-60-400	91.0 ± 2.5	274.2 ± 11.7	222.0 ± 11.8
PIF-60-500	96.8 ± 5.8	264.1 ± 20.5	217.6 ± 11.9
PIF-80-50	71.6 ± 2.1	278.3 ± 24.7	243.3 ± 15.8
PIF-80-100	89.5 ± 4.8	256.2 ± 22.3	175.1 ± 27.5
PIF-80-200	95.6 ± 9.1	274.2 ± 16.9	208.7 ± 28.5
PIF-80-300	97.7 ± 4.9	291.0 ± 22.8	185.8 ± 19.7
PIF-80-400	94.4 ± 4.1	304.0 ± 30.3.	191.3 ± 26.7